Available on the CERN CDS information server

CMS PAS SUS-12-009

CMS Physics Analysis Summary

Contact: cms-pag-conveners-susy@cern.ch

2012/07/05

A search for the decays of a new heavy particle in multijet events with the razor variables at CMS in pp collisions at $\sqrt{s} = 7TeV$

The CMS Collaboration

Abstract

A search is performed for the pair production of a new heavy resonance that decays into high jet-multiplicity final states with missing transverse energy using 4.98 ± 0.11 fb^{-1} of data collected by the CMS experiment in 2011 at the CERN Large Hadron Collider. The *razor* variables are used to study events with at least six jets, where at least one jet is identified as coming from the decay of a b-quark. These events are characterised by large M_R and small R^2 and are in a different kinematic region than previously studied. This analysis is sensitive to SUSY and SUSY-like signatures with the production of a high number of jets, such as top squark or t' pair production.

1 Introduction

Many frameworks for physics Beyond the Standard Model (BSM) include a "top partner", a heavy charge 2/3 colour triplet scalar or fermion. It is often assumed that this particle carries a nonzero value of some conserved exotic charge or parity, motivated either by a connection to dark matter or by the necessity to suppress effects in conflict with precision data [1]. In this case the top partner, denoted t', may decay predominantly to a top quark plus a neutral particle, denoted χ:

$$t' \to t + \chi \, , \tag{1}$$

where χ is not detected and may be a candidate for dark matter.

Examples of such top partners include fourth generation quarks with an extra quantum number related to dark matter [2] or to gauging baryon and lepton number [3]. Other such fermionic top partners occur in Little Higgs models with T-parity [4], and in generic models of Universal Extra Dimensions (UED) with conserved KK-parity [5]. We label these particles generically as $t'_{1/2}$. Scalar top partners with this type of decay, here denoted t'_0 but more usually top squarks, are a generic feature of supersymmetric models (SUSY) with conserved R-parity, provided that they are not too light [1]. In all cases the mass splitting between the top partner and the neutral decay product χ is not specified without further theoretical input; here, we take both $m_{t'}$ and m_χ to be free parameters, subject only to the constraint $m_{t'} > m_t + m_\chi$. Limits on spin-1/2 top partner quarks are thus simultaneously limits on a large class of fourth generation, Little Higgs, and UED models.

Both the CDF experiment at the Tevatron [6, 7] and the ATLAS experiment at the LHC [8] have searched for pair production of spin-1/2 top partner quarks, followed by the decay (1). These searches rely on detection of an electron or muon from a semileptonic top decay, and missing transverse energy from the two undetected χ particles.

Previous searches also constrain the direct pair production of top squarks in R-parity-conserving SUSY [9], but the production cross sections compared to the spin-1/2 top partners are supressed by a large factor: for 7 TeV pp collisions this factor varies between 6 (for $m_{t'_{1/2}} \simeq m_t$) and 12 (for $m_{t'_{1/2}} \simeq 1$ TeV). The main cause of this difference is the greater threshold suppression of the scalar pair production; the spin-1/2 versus scalar ratio grows with the mass of the top partner [10].

The search for the production and decay of t' pairs in the hadronic final state requires both a detailed understanding of the standard model (SM) background and the ability to separate signal and background. The focal point for the *razor* analysis [11–13] is the production of pairs of heavy particles, whose masses are significantly larger than those of any SM particle. The analysis is designed to kinematically discriminate the pair production of heavy particles from SM backgrounds, without making strong assumptions about the E_T^{miss} spectrum or details of the decay chains of these particles.

In this article, we present a complementary analysis to the *inclusive* razor analysis of the full 2011 dataset [14], in which the region of parameter space with low to intermediate intrinsic E_T^{miss} is probed. In order to access this region, a less inclusive selection must be considered; we require events to have at least 6 jets in the final state, of which at least one must be b-tagged, while also employing a lepton veto to remove most sources of genuine E_T^{miss}. The jets are grouped into two merged-jets to give a pseudo-dijet topology. The razor analysis then tests the consistency, event by event, of the hypothesis that the two merged jets represent the visible portion of the decays of two heavy particles. This approach should be model independent, while at the same time giving reasonable efficiency to select $t't'$ signal events, where both t' decay following Eq. 1, or SUSY-like events where gluinos are pair produced, and then decay like $\tilde{g} \to tt\chi$.

This strategy is complementary to traditional searches for signals in the tails of the $E_{\mathrm{T}}^{\mathrm{miss}}$ distribution [15–24] and is applied to data collected with the Compact Muon Solenoid (CMS) detector from pp collisions at $\sqrt{s} = 7\,\mathrm{TeV}$ corresponding to an integrated luminosity of $4.98\,\mathrm{fb}^{-1}$.

2 The CMS Apparatus

A description of the CMS detector can be found elsewhere [25]. A characteristic feature of the CMS detector is its superconducting solenoid magnet, of 6 m internal diameter, providing a field of 3.8 T. The silicon pixel and strip tracker, the crystal electromagnetic calorimeter (ECAL) and the brass/scintillator hadron calorimeter (HCAL) are contained within the solenoid. Muons are detected in gas-ionization chambers embedded in the steel return yoke. The ECAL has an energy resolution of better than 0.5 % above 100 GeV. The HCAL combined with the ECAL, measures the jet energy with a resolution $\Delta E/E \approx 100\,\%/\sqrt{E/\,\mathrm{GeV}} \oplus 5\,\%$.

CMS uses a coordinate system with the x-axis pointing towards the center of the LHC, the y-axis pointing up (perpendicular to the LHC plane), and the z-axis along the counterclockwise beam direction. The azimuthal angle ϕ is measured with respect to the x-axis in the xy plane and the polar angle θ is defined with respect to the z-axis. The pseudorapidity is $\eta = -\ln[\tan(\theta/2)]$.

3 The Razor Analysis

The razor kinematics are based on the generic process of the pair production of two heavy particles, each decaying to an unseen particle plus jets. This includes SUSY signals with complicated and varied decay chains, or the simplest case of a pair of squarks each decaying to a quark and the lightest supersymmetric particle (LSP). All such processes are treated on an equal footing by forcing every event into a dijet topology; this is done by combining all jets in the event into two merged jets. All leptons are included in the jets, however, events featuring isolated leptons are removed from the search dataset.

To the extent that the pair of merged jets accurately reconstruct the visible portion of the underlying parent particle decays, the signal kinematics is equivalent to pair production of heavy squarks $\tilde{q}_1$, $\tilde{q}_2$, with $\tilde{q}_i \to \mathrm{j}_i\tilde{\chi}_i$, where the $\tilde{\chi}_i$ are LSPs and j_i denotes the visible products of the decays. We assume that the squarks have the same mass and, for simplicity, we will use the approximation that the j_i are massless.

The standard computation of the cross section for such a process uses a parameterization of the phase space and the matrix element extracted from consideration of three preferred reference frames: the rest frames of the two squarks and the center of mass (CM) frame.

In the rest frame of the ith squark, the 4-momenta of the squark and its decay products have the simple form:

$$
\begin{aligned}
p_{\tilde{q}_i} &= M_{\tilde{q}}(1,0)\ , &(2)\\
p_{\mathrm{j}_i} &= \frac{M_\Delta}{2}(1,\hat{u}_i)\ , &(3)\\
p_{\chi_i} &= \frac{M_\Delta}{2}(\frac{1}{\beta_\Delta},-\hat{u}_i)\ , &(4)
\end{aligned}
$$

where the $\hat{u}_i$ are unit vectors in the directions of the visible decay products,

$$
M_\Delta \equiv \frac{M_{\tilde{q}}^2 - M_{\tilde{\chi}}^2}{M_{\tilde{q}}} = 2M_{\tilde{\chi}}\gamma_\Delta\beta_\Delta\ , \tag{5}
$$

and β_Δ is the boost parameter to the rest frame of the LSP $\tilde{\chi}_i$. The other preferred frame is the $\tilde{q}_1\tilde{q}_2$ CM frame, with

$$
\begin{aligned}
p'_{\tilde{q}_1} &= \gamma_{CM}M_{\tilde{q}}\,(1,\ \beta_{CM}\hat{u}_{\tilde{q}})\ , &(6)\\
p'_{\tilde{q}_2} &= \gamma_{CM}M_{\tilde{q}}\,(1,-\beta_{CM}\hat{u}_{\tilde{q}})\ , &(7)
\end{aligned}
$$

where $\hat{u}_{\tilde{q}}$ is a unit vector in the direction of the first squark, and β_{CM} is the boost parameter from the CM frame to the $\tilde{q}_1$ rest frame. In the CM frame the energies of the visible decay products can be written as follows:

$$
\begin{aligned}
E_{\mathrm{j}_1} &= \frac{\gamma_{CM}M_\Delta}{2}(1+\beta_{CM}\hat{u}_{\tilde{q}}\cdot\hat{u}_1)\ , &(8)\\
E_{\mathrm{j}_2} &= \frac{\gamma_{CM}M_\Delta}{2}(1+\beta_{CM}\hat{u}_{\tilde{q}}\cdot\hat{u}_2)\ . &(9)
\end{aligned}
$$

Since the second term typically averages to zero, the energy distribution for the visible decay products as measured in the CM frame peaks around $(\gamma_{CM}M_\Delta)/2$.

The problem with the conventional parameterization of this process is that, with two unseen particles, there are not enough experimental observables to reconstruct any of the three reference frames just described. This is true even in the absence of initial state p_T (as will now be assumed throughout), where the CM frame is just a longitudinal boost from the lab frame.

The strategy of the razor analysis is to approximate these unknown frames with a razor frame that is defined unambiguously from measured quantities in the lab frame. Event by event, razor frame observables then estimate the scales M_Δ and $\gamma_{CM}M_\Delta$ seen above.

A razor frame is defined by finding a longitudinal boost from the lab frame to a frame where the visible energies can be written in terms of an overall scale that is manifestly invariant under longitudinal boosts. This then defines a razor frame where the scale of the visible energies is set by a quantity that should approximate $\gamma_{CM}M_\Delta$ in the (unknown) CM frame. The longitudinal boost used here is defined as:

$$
\beta_L^R \equiv \frac{p_z^{\mathrm{j}_1} + p_z^{\mathrm{j}_2}}{E_{\mathrm{j}_1} + E_{\mathrm{j}_2}}\ . \tag{10}
$$

The razor boost β_L^R defines a frame where the visible four-momenta reduce to

$$p_{\mathrm{j}_1} = (\frac{1}{2}(M_R - \frac{(\vec{p}_T^{\,\mathrm{j}_1} - \vec{p}_T^{\,\mathrm{j}_2}) \cdot \vec{E}_T^{miss}}{M_R}), p_T^{\mathrm{j}_1}, p_z) , \tag{11}$$

$$p_{\mathrm{j}_2} = (\frac{1}{2}(M_R + \frac{(\vec{p}_T^{\,\mathrm{j}_1} - \vec{p}_T^{\,\mathrm{j}_2}) \cdot \vec{E}_T^{miss}}{M_R}), p_T^{\mathrm{j}_2}, -p_z) , \tag{12}$$

where M_R is the longitudinal boost invariant

$$M_R \equiv \sqrt{(E_{\mathrm{j}_1} + E_{\mathrm{j}_2})^2 - (p_z^{\mathrm{j}_1} + p_z^{\mathrm{j}_2})^2} , \tag{13}$$

and the longitudinal momentum p_z is determined from the massless on-shell conditions. This frame always exists since the magnitude of β_L^R is less than unity. This definition of M_R is enhanced with respect to the one used in [12] to avoid configurations where M_R is ill-defined due to unphysical Lorentz transformations. Here M_R as defined by (13) is an estimator of $\gamma_{CM} M_\Delta$.

The next step of the razor strategy is to define a transverse observable that can also serve as an event-by-event estimator of the underlying scale M_Δ. As usual for transverse quantities we expect M_Δ to be related to a kinematic edge rather than a peak.

Several choices of the transverse observable are plausible. To the extent that events match the assumed topology, the maximum value of the scalar sum of the merged jets transverse momenta (p_T^1, p_T^2) is M_Δ. The maximum value of the E_T^{miss} is also M_Δ. Especially useful is M_T^R, a kind of average transverse mass whose maximum value for signal events is also M_Δ:

$$M_T^R \equiv \sqrt{\frac{E_T^{miss}(p_T^{j1} + p_T^{j2}) - \vec{E}_T^{miss} \cdot (\vec{p}_T^{\,j1} + \vec{p}_T^{\,j2})}{2}} . \tag{14}$$

Given a global estimator M_R and a transverse estimator M_T^R, the razor dimensionless ratio is defined as

$$R \equiv \frac{M_T^R}{M_R} . \tag{15}$$

Signal events are characterized by the heavy scale M_Δ, while backgrounds are not. Qualitatively we expect M_R to peak for the signal over a steeply falling background. Thus the search for an excess of signal events in a tail of a distribution is recast as a search for a peak on top of a steeply falling SM residual tail.

To extract the peaking signal we need first to reduce the QCD multijet background to manageable levels. This is achieved by imposing a threshold value for R. However, since we are aiming to gain sensitivity to models where the LSP is light, this threshold cannot be too high and we must live with some QCD contamination.

For signal events M_T^R has a maximum value of M_Δ (i.e. a kinematic edge); thus R has a maximum value of approximately one and the distribution of R for signal peaks around 0.6, in contrast to QCD multijet events which peak at zero. These properties motivate the appropriate kinematic requirements for the signal selection and background reduction. We note that, while M_T^R and M_R measure the same scale (one as an end-point the other as a peak), they are largely uncorrelated for signal events [12].

4 Analysis path

In both simulation and data, the distributions of SM background events are seen to have a simple exponential dependence on the razor variables R and M_R over a large fraction of the R^2-M_R plane. The analysis uses both simulated events and two independent data control samples to understand the shapes of the SM background distributions, the number of independent parameters needed to describe them, and to extract initial estimates of the values of these parameters.

We model the overall SM background distribution as a linear sum of two distributions describing the major backgrounds; QCD multijet and $t\bar{t}$. A data control sample, where events with a b-tagged jet are vetoed, is used to estimate the shape of these two backgrounds with an unbinned maximum likelihood (ML) fit. The exact parameters describing these two distributions, as well as their relative normalisations, are then extracted using a fit to the ≥ 1 b-tag sample in a region of the M_R-R^2 with a low expected signal to background ratio. This distribution is extrapolated to an orthogonal region of the R^2-M_R plane, defined such that the two regions overlap when projected on either one of the axes (R^2 or M_R).

The main steps in the analysis path are outlined below.

Definition of data samples

1. Inclusive data sets are collected with the CMS multijet triggers requiring at least 4, 6, or 8 high p_T jets.

2. The datasets are processed to minimise the effects from pileup and detector noise. Events with less than 6 inclusive jets are removed.

3. The remaining events are split into three disjoint boxes depending on the number of b-jets, identified with the track-counting high efficiency (TCHE) algorithm, and the number of isolated leptons, including taus.

4. The events with zero jets passing the TCHE loose working point and zero isolated leptons go into the BVeto box, while those with one isolated lepton enter the LeptonBVeto box. These boxes are almost signal free control regions from which the shapes of the QCD multijet and W+jets (similar in shape to semileptonic $t\bar{t}$ at high jet multiplicities) backgrounds can be extracted.

5. Events with at least one jet passing the TCHE medium working point and no isolated leptons go into the BJet box, in which the search is performed. The majority of hadronically decaying signal is expected in this box.

Fitting and extrapolation to signal regions

1. The data is studied for each box in the R^2 –M_R plane. We apply a baseline requirement so that the kinematic turn on seen in both variables is removed and we are left with the exponential tail. We consider events with $500 \leq M_R \leq 4000$ GeV and $0.03 \leq R^2 \leq 1.0$. The lower cut on R^2 is already very effective at removing QCD and should be contrasted with the value of 0.18 from the inclusive razor analysis.

2. The background shape describing events from leptonic $t\bar{t}$ and W+jets decays is extracted using an unbinned ML fit to all events in the LeptonBVeto box, with initial parameter estimates taken from Monte Carlo (MC). The parameters found by the fit are then propagated to the other boxes, multiplying the likelihood by Gaussian penalty terms. Each

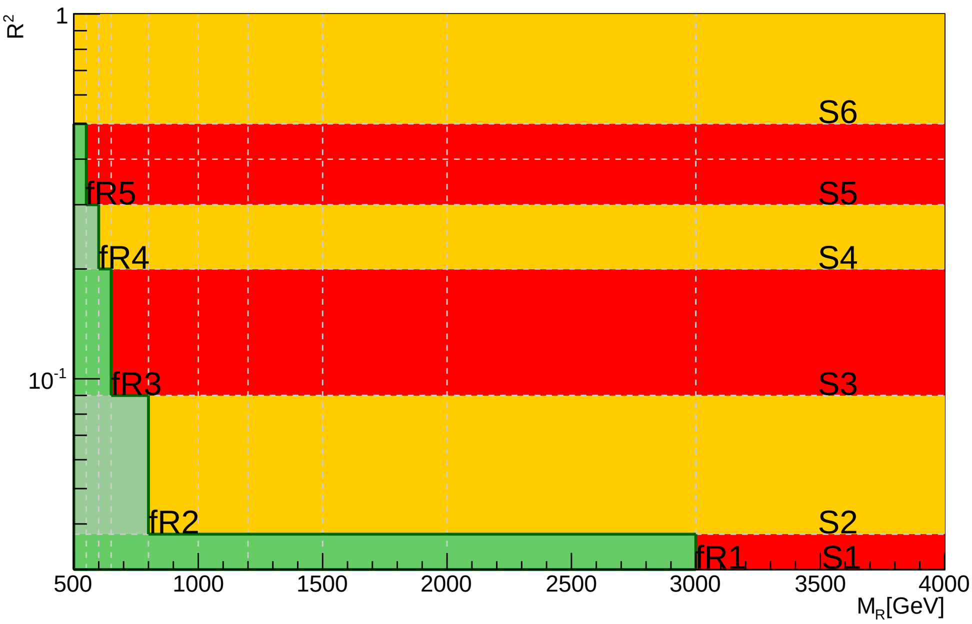

Figure 1: The M_R-R^2 plane is sub-divided into five fit regions (fR_i), shown in green, and six adjacent signal regions (S_i) (red or orange). Data in the fit region (the sum of the all fR_i are used to extract a background model. The signal regions are then used to establish the agreement between this model and the data in a region excluded from the fit.

penalty is centred around the value extracted with the width set to the uncertainty from the fit.

3. The QCD background shape is then extracted by fitting all data in the BVeto box and the QCD-like shape propagated to the BJet box. The initial parameter estimates for the QCD shape are taken from MC.

4. We define a *fit region* in the bottom-left corner of the BJet box (see Fig. 1), where the number of signal events expected is small compared to the SM background. The areas excluded from the fit region are expected to have higher sensitivity to potential signal events.

5. We fit the events in the fit region under the background-only hypothesis to derive a model for the shape and yields of the SM backgrounds. We then use this background model to extrapolate to the rest of the analysis region in the $R^2 - M_R$ plane. The MC dependence on the final background shape has been shown to be negligible. We quantify the agreement between the data and the background model through the integral of the background model yield in a limited set of predefined non-overlapping *signal regions* (SRs), shown in Fig. 1, motivated by MC studies.

6. Observing no significant excess we proceed to set limits using a hybrid CL_s [26] test on the full R^2-M_R plane. We use a finer binning of the 2D plane to build a numerical probability density function (PDF) of the signal distribution for a given signal model.

Each of these steps is described in more detail later.

5 Monte Carlo Event Samples

The design of the analysis was guided by studies of MC event samples generated with the PYTHIA6 [27] and MADGRAPH V4.22 [28] programs, simulated using the CMS GEANT-based [29] detector simulation, and then processed by the same software used to reconstruct real collision data. Events with top quarks and electroweak bosons where generated with MADGRAPH interfaced with PYTHIA for parton showering, hadronization and the underlying event description, while the QCD multijet sample was generated with PYTHIA alone with the requirement that there be at least 6 jets at generator level.

For the model dependent results, presented in Sec. 10, we use signal MC generated to match the topology of the `T2tt` simplified model (SMS). In simplified models, introduced in Refs. [30, 31], a limited set of hypothetical particles and decay chains are defined to describe a given topological signature. Specific applications of these ideas have appeared in Refs. [32–36]. The `T2tt` model describes the topology $pp \to t't'; t' \to t\chi$. The spin of the t' is 0 in the MC (denoted t'_0 in the text), corresponding to the SUSY top squark, however we also consider the spin-1/2 partner, denoted $t'_{1/2}$, as explained in section 1. A second SMS model, `T1tttt`, is also investigated. This model describes the pair-production and decay of the SUSY gluino in the case where it is much lighter than the top squark. The decay topology is then $pp \to \tilde{g}\tilde{g}; \tilde{g} \to 2t + \tilde{\chi}$.

To generate SMS MC samples, the mass spectrum was first calculated with SOFTSUSY [37] and the decays with SUSYHIT[38]. The PYTHIA program was used with the SLHA interface [39] to generate the events, which were then processed with a fast simulation of the CMS detector. The generator-level cross section and the k-factors for the Next-to-Leading Order and Next-to-Leading Logs (NLO+NLL) SUSY t'_0 cross section calculation [40], and then rescaled with a leading order (LO) k-factor [10, 41] in order to obtain the $t'_{1/2}$ cross-section. The same signal MC is used for both the t'_0 and $t'_{1/2}$ results; differences in the selection efficiencies due to spin effects are expected to be small. For the `T1tttt` model, only the NLO+NLL SUSY gluino cross-section was considered.

6 Event Selection

Events are required to have at least one good reconstructed interaction vertex [42]. When multiple vertices are found, the one with the highest associated $\sum_{track} p_T^2$ is used. Jets are reconstructed offline from calorimeter energy deposits and tracks, associated with the particle-flow algorithm, using the infrared-safe anti-k_T [43] algorithm with radius parameter 0.5. Jets are corrected for the non-uniformity of the calorimeter response in energy and η using MC and data derived corrections and are required to have $p_T > 30$ GeV and $|\eta| < 3.0$. Further corrections are applied to minimise the effect of pileup. We require 6 jets in the event, of which at least 2 must have a higher p_T of 80 GeV. The E_T^{miss} is also reconstructed using the particle-flow algorithm [44].

Events are first categorised by the number of jets identified as coming from a b-quark, using the TCHE algorithm [45]. Those events with no jets passing the loose working point may enter the LeptonBVeto or BVeto boxes, while those with at least one jet passing the medium working point may enter the BJet box.

Events containing isolated leptons, again reconstructed with the particle-flow algorithm are vetoed from the BJet and BVeto boxes, but retained in the LeptonBVeto box. The isolation criteria are pileup protected by subtracting the contribution from charged hadrons identified as coming from pileup vertexes lying within the isolation cone. The electron and muon identification criteria are described in [46], while the tau identification is described in [47]. In each case, a looser identification without isolation is also considered in order to monitor the effect that the remaining leptons have on the background shapes.

The reconstructed jets, which also contain any leptons present, are grouped into two merged jets. The merged jets are constructed as a sum of the four-momenta of their constituent objects. After considering all possible partitions of the objects into two merged jets, the combination minimizing the invariant masses summed in quadrature of the resulting merged jets is selected. Finally, the razor variables are calculated and events with $M_R < 500$ GeV or $R^2 < 0.03$ are removed. The final selection efficiencies for the `T2tt` SMS MC for each box is shown in Appendix A and for `T1tttt` in Appendix B.

7 Background Determination

We perform an extended and unbinned ML fit, using the ROOFIT software package [48]. For the LeptonBVeto and BVeto boxes the full R^2-M_R plane is used, while in the BJet box, the fit is performed in the portion of the plane delimited by the green contours, shown in Fig. 1. We refer to this region as the *fit region*. The fit provides a full description of the SM background in the R^2-M_R plane in each box. The likelihood function for a given box is written as [49]:

$$\mathcal{L}_b = \frac{e^{-(\sum_{j\in SM} N_j)}}{N!} \prod_{i=1}^{N} \Big(\sum_{j\in SM} N_j P_j(M_{R,i}, R_i^2) \Big) \,, \tag{16}$$

where N is the total number of events in the box; the sum runs on all the SM processes (QCD and $t\bar{t}$), N_j is the yield of a given fit sample in the box, and $P_j(M_R, R^2)$ is the two-dimensional PDF describing the R^2 versus M_R distribution of the considered process.

The P_j function is written as the sum of two instances of the same function (two *components*)

$$P_j(M_R, R^2) = (1 - f_2^j) \times F_j^{1st}(M_R, R^2) + f_2^j \times F_j^{2nd}(M_R, R^2) \,, \tag{17}$$

where f_2^j is the relative fraction of the second component and each component is written as:

$$F_j(M_R, R^2) = \Big[k_j(M_R - M_{R,j}^0)(R^2 - R_{0,j}^2) - 1 \Big] \, e^{-k_j(M_R - M_{R,j}^0)(R^2 - R_{0,j}^2)} \,. \tag{18}$$

When integrated on M_R (R^2), this function recovers the exponential behaviour on R^2 (M_R).

While the shape of the first component is in general box dependent, the second component is found to be box independent in simulation studies as well as in fits to control data samples in the inclusive analysis. This behaviour is found to be associated with large initial state radiation (ISR).

QCD and $t\bar{t}$ MC are first used to obtain an estimate of the background parameters in the LeptonBVeto and BVeto boxes. The relevant shapes are then extracted from these data control regions, as described in section 4. These parameters are propagated to the BJet box, drastically reducing the dependence on MC. The values of the shape parameters that maximize the likelihood in these fits, along with the corresponding covariance matrix, are used to define the background model and the uncertainty associated to it. One dimensional projections of the data and the fit result are shown in Fig. 2 for M_R and R^2.

The multijet triggers used to select the data events are not 100% efficient in the low M_R part of the fit region and this induces a shape variation in the first component that is not modelled by the fit. While this leads to a systematic over-prediction of the background in the turn-on region, extensive studies have confirmed that the second component, which drives the background prediction in the signal regions, is unaffected. This allows a loose selection to be used offline without trying to remove the trigger turn-on region.

Once the background shape parameterization is determined, it is used to estimate the total SM background yield in regions where new physics signal would be visible. In the absence of such a signal, the background shape is used to constrain the parameters of the new physics model under consideration.

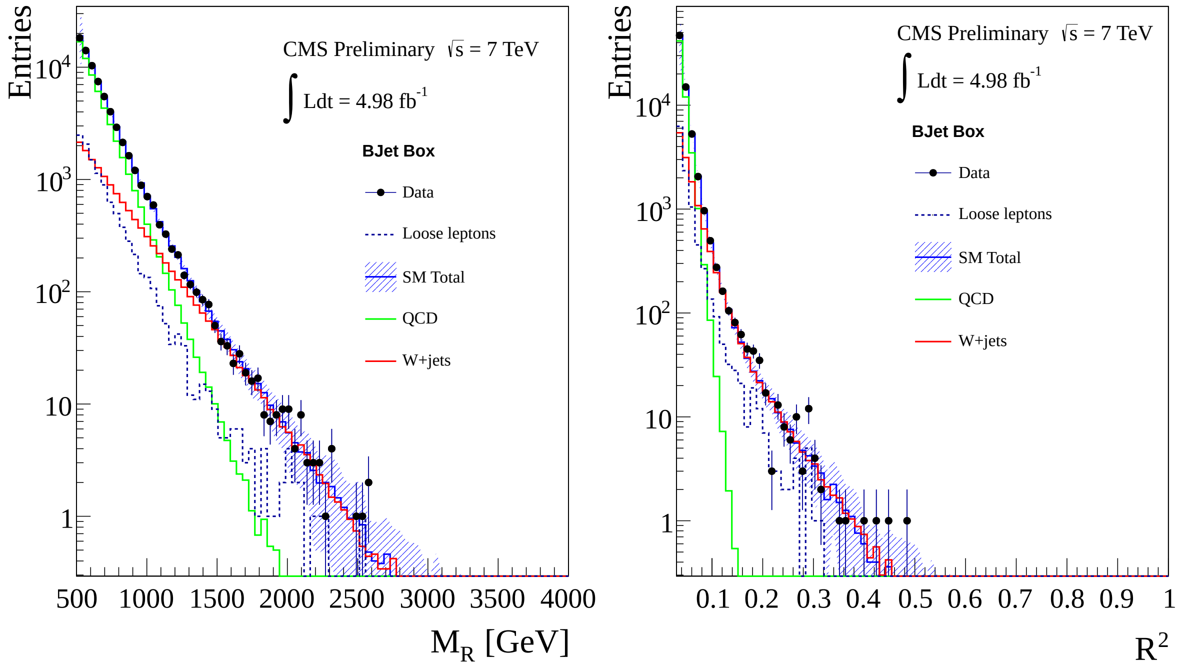

Figure 2: Projection of the 2D fit result on M_R (left) and R^2 (right) for the BJet box using the full 2011 CMS MultiJet dataset. The blue histogram is the total SM prediction as obtained from a single large pseudo-experiment based on the 2D fit, while the histogram uncertainties show the 68% range from the covariance matrix. The breakdown of the different background components is also shown. The fit is performed in the R^2-M_R sideband and projected into the full region to allow comparison between the prediction from the fit and the data.

8 Signal Regions

In order to establish the compatibility of the background model to the observed dataset, we define a set of SR on the tail of the background distribution.

The SR are chosen before looking at the data, based on the prediction of the background model obtained by MC simulation. The SR are defined such that full populated range of M_R values (after the event selection) is covered. Different requirements on R^2 are used in different SR, such that the expected background yield is kept small. The defined SR are shown in Fig. 1.

Using the background model returned by the ML fit, we derive the distribution of the expected yield in each SR using pseudo-experiments. In order to correctly account for correlations and uncertainties on the parameters describing the background model, the shape parameters used to generate each pseudo-experiment dataset are sampled from the covariance matrix returned by the ML fit. The actual number of events in each dataset is then drawn from a Poisson distribution centred on the yield returned by the covariance-matrix sampling. For each pseudo-experiment dataset, the number of events in the SR is found. For each of the SR, the distribution of the number of events derived by the pseudo-experiments is used to calculate a two-sided p-value, corresponding to the probability of observing an equal or less probable outcome for a counting experiment in each SR. The p-values obtained are quoted in Tab. 1. In the same table, we quote the median and the mode of the yield distribution for each SR, together with the observed yield. A 68% probability interval is also calculated, using the probability associated to each yield outcome as the ordering principle.

Region	M_R	R^2	Observed	Predicted Mode	Predicted Median	Predicted 68 Prob. Range	p-value
S_1	$[3000, 4000]$	$[0.0300, 0.0375]$	0	0.5	0.5	2.5 ± 2.5	0.99
S_2	$[800, 4000]$	$[0.0375, 0.0900]$	4328	4318.5	3709.5	4426.5 ± 718.5	0.40
S_3	$[650, 4000]$	$[0.0900, 0.2000]$	551	504.5	500.5	640.5 ± 140.5	0.43
S_4	$[600, 4000]$	$[0.2000, 0.3000]$	37	33.5	11.5	37.0 ± 27.0	0.84
S_5	$[550, 4000]$	$[0.3000, 0.5000]$	7	9.5	1.5	14.0 ± 14.0	0.70
S_6	$[500, 4000]$	$[0.5000, 1.0000]$	0	0.5	0.5	3.0 ± 3.0	0.99

Table 1: Agreement between observed yield and expected background in the S_i regions, obtained integrating numerically the background model (including shape uncertainties) with toy MC. The signal regions are shown in Fig. 1.

No significant deviation is observed, which indicates the compatibility of the background model to the data and the absence of a significant excess from non-SM processes.

9 Interpretation of the Results

We interpret our result as an exclusion limit at 95% confidence level (CL) in the $m_{t'}$ versus m_{LSP} plane for the `T2tt` SMS and the $m_{\tilde{g}}$ versus m_{LSP} plane for the `T1tttt` SMS.

We scan the parameter space and perform a hypothesis test. There are two well-specified situations under consideration: either the background only hypothesis (H_0) is enough to model the data, or we must include a signal component (H_1) in order to correctly model the distribution seen in data. In the absence of a significant deviation from our background model, we associate a CL to the rejection of H_1 in favour of H_0, computing the value of the hybrid CL_s [26] for that model point.

Each hypothesis is represented as a likelihood function. The hypothesis H_0 is associated to the likelihood function of Eq. 16, while the likelihood function associated to H_1 is written as:

$$\mathcal{L}_{s+b} = \frac{e^{-N_S - (\sum_{j \in SM} N_j)}}{N!} \prod_{i=1}^{N} (N_S P_S(M_{R,i}, R_i^2) + \sum_{j \in SM} N_j P_j(M_{R,i}, R_i^2)) \,, \tag{19}$$

where the background parameters N_j and the PDF's $P_j(M_R, R^2)$ are the same as in Eq. 16; N_S is the expected signal yield, and $P_S(M_R, R^2)$ is the PDF associated to the model-point, parameterized as a 2D template function using fast MC simulation. We use variable binning in M_R, shown in Fig. 1, to further avoid sparse signal PDFs at larger M_R. The value of N_S in each box is computed from a model independent cross section of the considered SMS point, the nominal integrated luminosity value corresponding to the dataset, and the reconstruction efficiency for the considered model point, evaluated using MC simulation. The model independent cross-sections considered were: $[10, 5, 1, 0.5, 0.1, 0.05, 0.01, 0.001]$ pb.

We consider the test statistics given by the logarithm of the likelihood ratio $\ln Q = \ln \frac{\mathcal{L}(s+b|H)}{\mathcal{L}(b|H)}$, where H is the hypothesis under test H_1 (signal plus background) or the null hypothesis H_0 (background-only). For a given dataset, we evaluate $\ln Q$ in the full region of events passing the baseline selection, excluding only the events belonging to the *fit region*.

Assuming the validity of H_0, the distribution of $\ln Q$ is derived from an ensemble of background-only pseudo-experiments, following the same procedure as described in Sec. 8. Alternative functional forms for the background model were investigated, however, for the family of functions that describe the data, the effect of changing the background description was negligible compared to the uncertainty on the central background model due to the covariance matrix.

We determine the distribution of $\ln Q$ under the assumption of H_1 by sampling pseudo-experiment datasets out of the likelihood function of Eq. 19. As for the background-only pseudo-experiments, the background model for each generation is derived from the covariance matrix returned by the ML fit.

Similarly, the signal PDF is varied *at generation* in each pseudo-experiment, in order to take into account the systematic uncertainties associated to the normalization and the shape of the signal distribution. We consider effects across the R^2– M_R plane that coherently affect the overall normalization, as well as systematic effects that vary across the R^2–M_R plane and between final state boxes which can affect the signal PDF shape. Bin-by-bin, the total systematic error on the $P_S(M_R, R^2)$ function of Eq. 19 is the convolution of the individual effects each modelled with a log-normal function. The systematic effects on the signal yield and the the signal shape modelling are summarized in Table 2. We consider variations of the function modelling the signal uncertainty (log-normal vs Gaussian) as well as the binning finding negligible deviations in the result.

While the systematic uncertainties are included when sampling the pseudo-experiments, the likelihood values are computed taking the nominal values for the shape and normalization parameters for both the background and signal PDF's.

Given the distribution of $\ln Q$ for background-only and signal-plus-background pseudo-experiments, the value of $\ln Q$ observed in the data $\ln Q^{\text{data}}$ determines the two tail regions, the integral of which yields the values of CL_{s+b} and $1 - CL_b$. From these values we compute $CL_s = CL_{s+b}/CL_b$. These CL_s values are used to set a limit in the SMS plane, excluding models at 95% CL if $CL_s < 0.05$, by extrapolating the CL_s values from each of the model independent cross-sections using the error function. The result is shown in Figure 3 for the `T2tt` and Figure 4 for the `T1tttt`.

Table 2: Summary of the systematic uncertainties on the signal yield and shape. The yield systematics are overall normalization factors, independent of the specific model considered. The shape systematics depend on the specific signal model, as well as on the considered region of the R^2 vs. M_R plane (point-by-point).

yield systematics	
$\mathcal{L}$	2.2%
MC Trigger emulation	5%
Tau ID data/MC efficiency	2%
shape systematics	
B-tag data/MC efficiency	point-by-point $\mathcal{O}(2\%) - \mathcal{O}(5\%)$
Parton Distribution Functions	point-by-point $\mathcal{O}(10\%) - \mathcal{O}(70\%)$
Jet Energy Scale	point-by-point $\mathcal{O}(5\%) - \mathcal{O}(20\%)$

10 Summary

We performed an inclusive search for new physic in the hadronic six jets + b-tag final state using $4.98 \pm 0.11\,\mathrm{fb}^{-1}$ of integrated luminosity from pp collisions at $\sqrt{s} = 7\,\mathrm{TeV}$, recorded by the CMS detector at the LHC. The kinematic consistency of the selected events was tested against the hypothesis of heavy particle pair production using the dimensionless razor variable R related to the missing transverse energy $E_{\mathrm{T}}^{\mathrm{miss}}$, and M_R, an event-by-event indicator of the heavy particle mass scale. No significant excess over the background expectations was observed and the results were presented as a 95% CL in the ($m_{t'}$, m_{LSP}) SMS `T2tt` and ($m_{\tilde{g}}$, m_{LSP}) SMS `T1tttt` parameter spaces. These results improve the limits for regions with low average values of R^2 and medium M_R when compared to the Razor inclusive analysis, and allow the exclusion of models in which $t'_{1/2}$ are produced in pairs and then decay $t' \to t\chi$ for t' masses $\lesssim$ 750 GeV. Models in which gluinos are pair-produced and then decay $\tilde{g} \to tt\tilde{\chi}$ are also excluded for gluino masses $\lesssim$ 900 GeV. Fig. 5 shows this explicitly, comparing the theoretical cross-sections with the expected and observed exclusion limits as a function of the t' or gluino mass, for a fixed LSP mass (50 GeV).

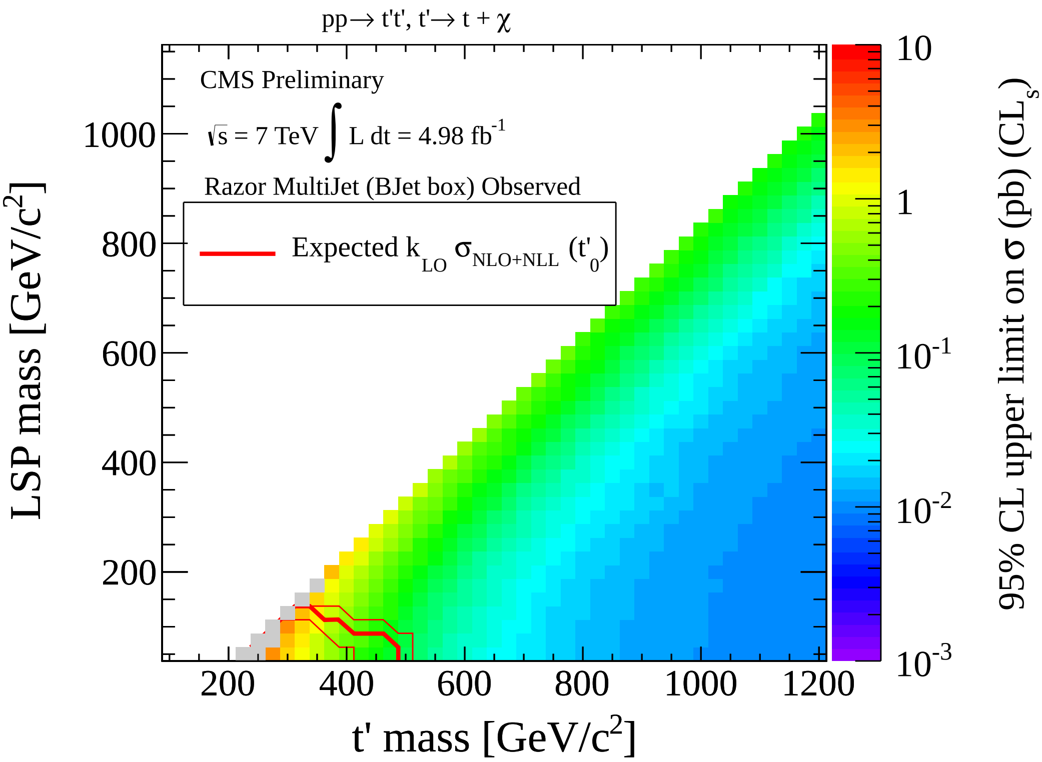

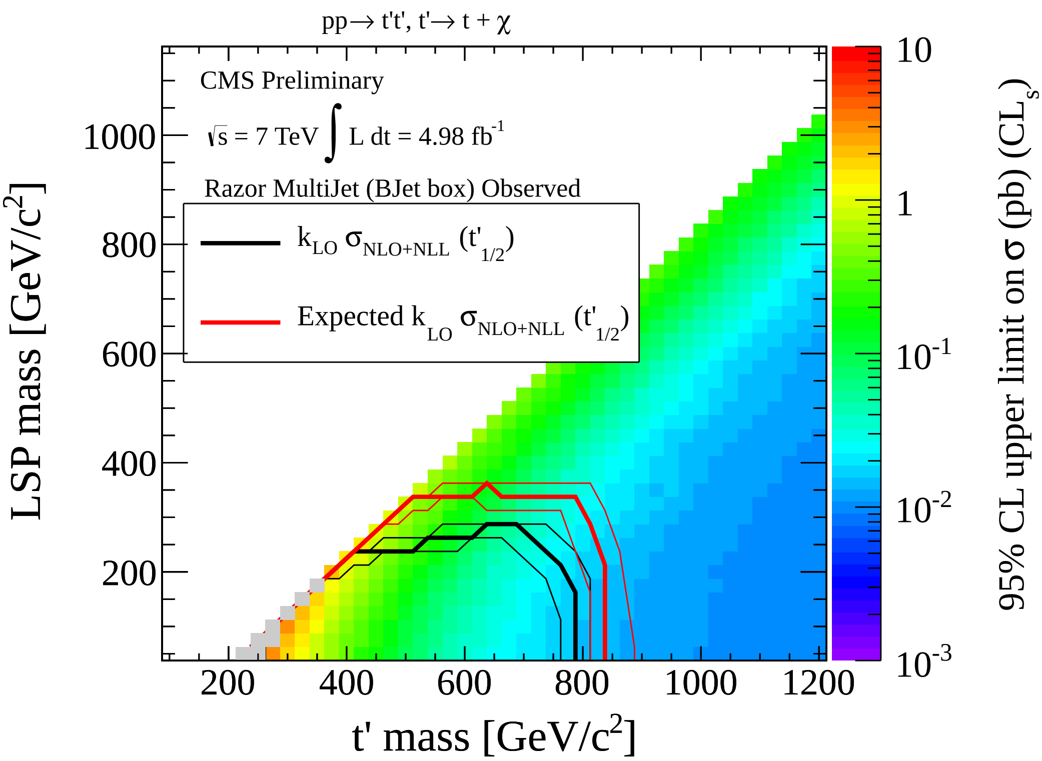

Figure 3: Expected and observed 95% CL limits in the ($m_{t'}$, m_{LSP}) SMS `T2tt` plane from the razor multijet analysis as derived from the BJet box. The black (red) lines show the observed (expected) limit for the t'_0 (top) and the $t'_{1/2}$ (bottom). The theoretical uncertainties arising from scale and parton distribution function uncertainties are also shown by the narrow lines. The colour scale shows the model independent cross-section excluded in this SMS. The solid grey region indicates model points where the analysis was found to have dependence on initial state radiation modelling in the simulation of signal events above a pre-defined tolerance; no interpretation is presented for these model points.

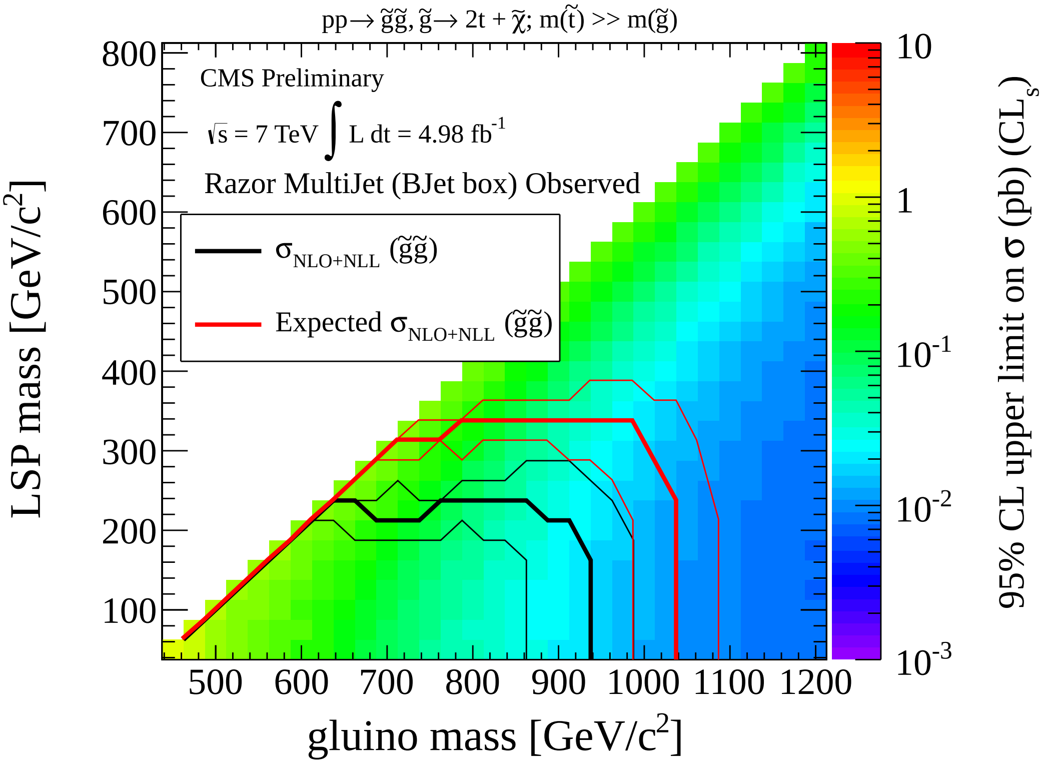

Figure 4: Expected and observed 95% CL limits in the ($m_{\tilde{g}}$, m_{LSP}) SMS `T1tttt` plane from the razor multijet analysis as derived from the BJet box. The black (red) lines shows the observed (expected) limit for the production of gluino pairs in SUSY. The theoretical uncertainties arising from scale and and parton distribution function uncertainties are also shown. The colour scale shows the model independent cross-section excluded in this SMS. No model points where the analysis was seen to have dependence on initial state radiation modelling in the simulation of signal events above a pre-defined tolerance were found.

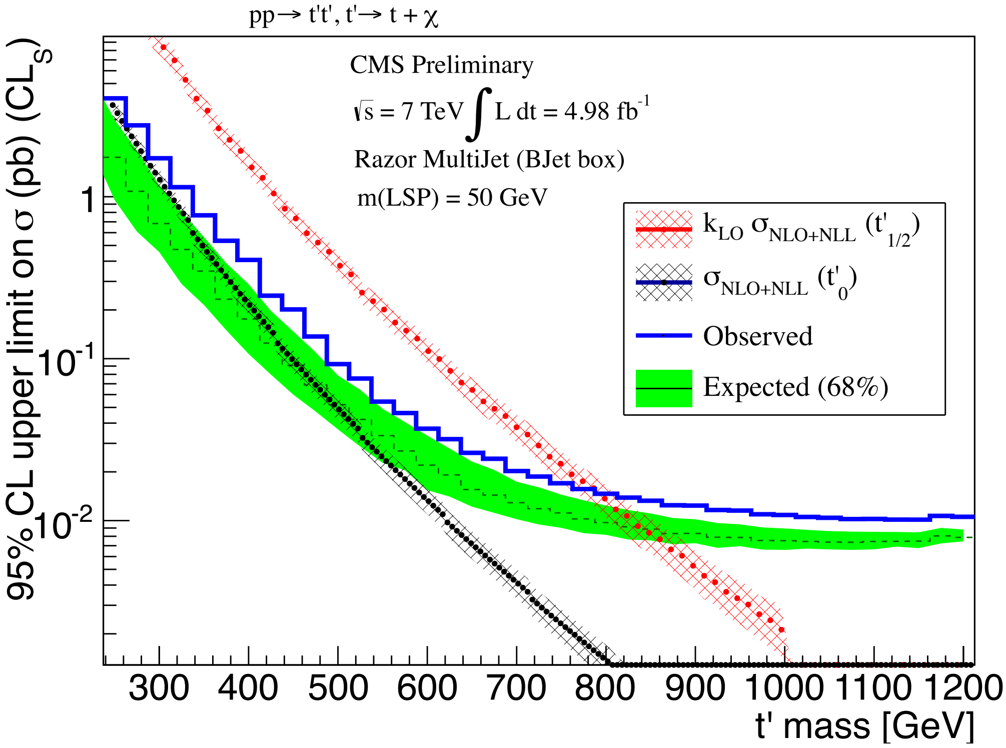

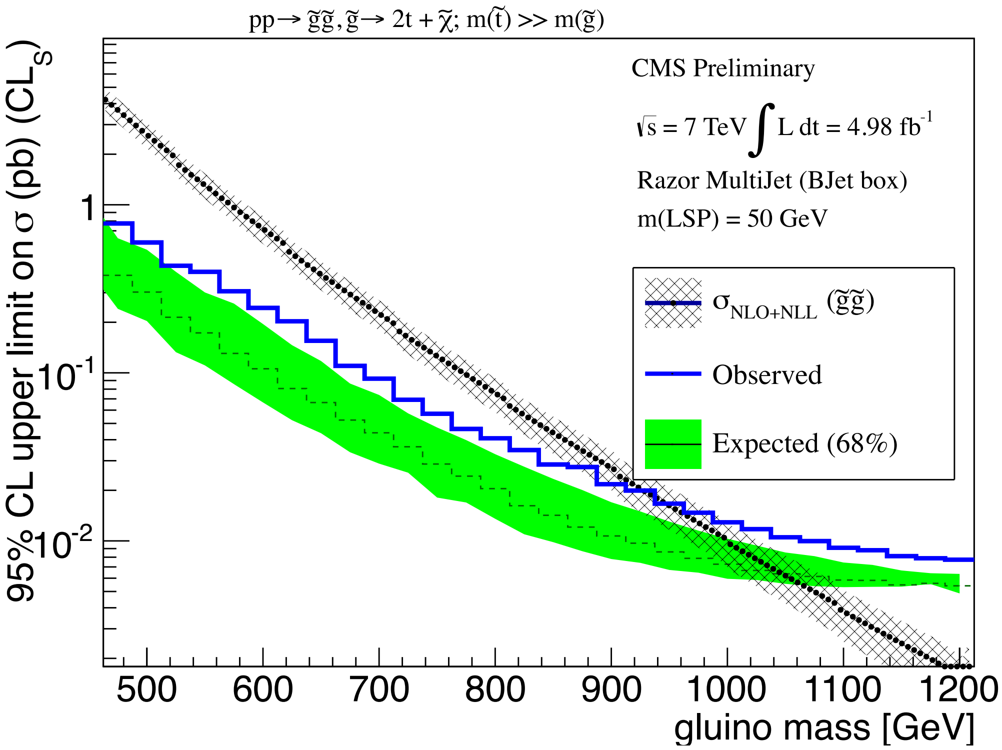

Figure 5: Expected and observed limits for `T2tt` (top) and `T1tttt` (bottom) with the LSP mass fixed to 50 GeV. In each case, the relevant theoretical cross-sections and uncertainties are shown.

A T2tt Simplified Model Efficiencies

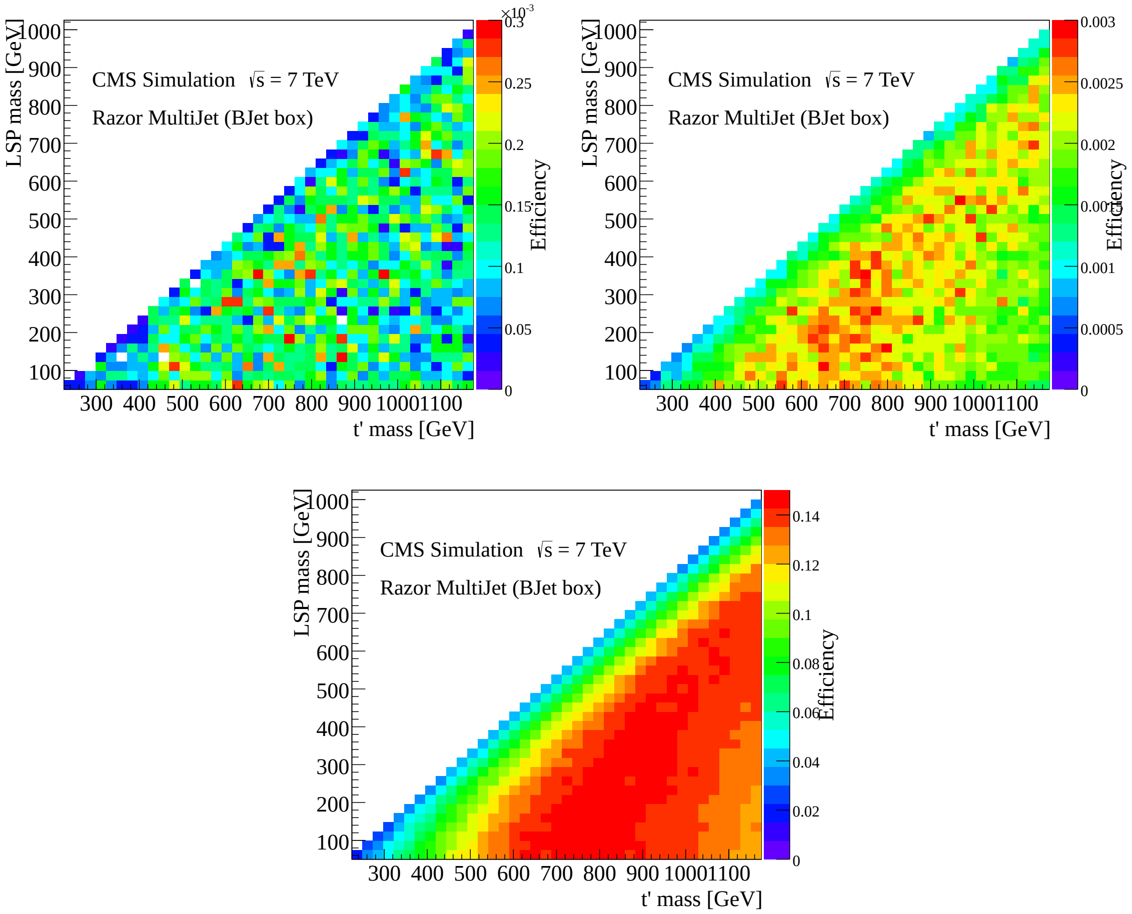

Figure 6: Top: Signal MC efficiencies, relative to the total number of events per SMS point, for the LeptonBVeto (top left), BVeto (top right), and BJet (bottom) boxes as a function of the SMS `T2tt` model parameters. It can be seen that the signal efficiency in the two data control regions is very low.

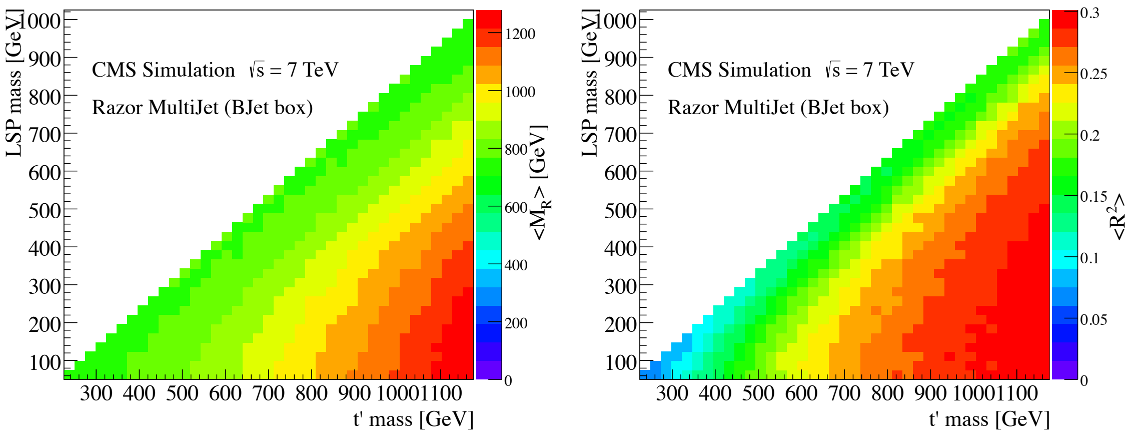

Figure 7: Average values of M_R (left) and R^2 (right) for the BJet box as a function of the SMS `T2tt` parameters.

B T1tttt Simplified Model Efficiencies

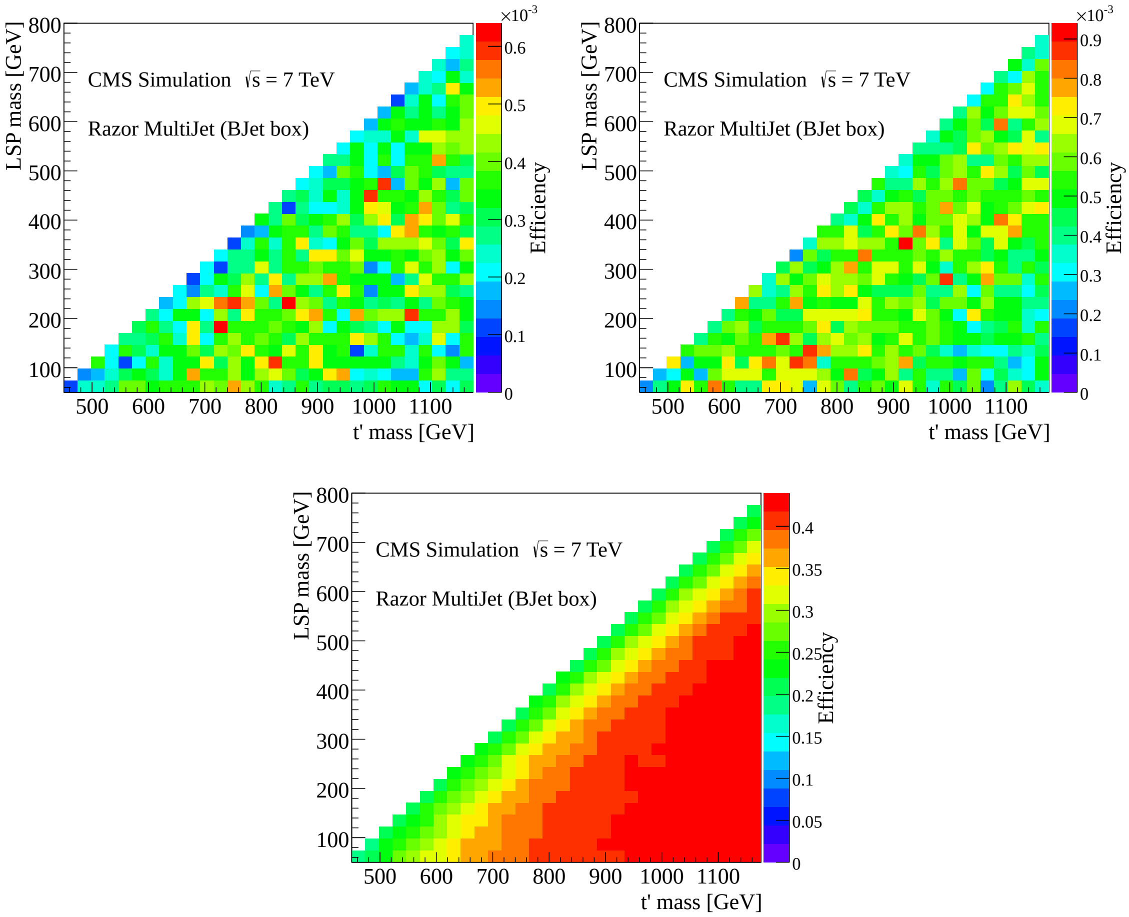

Figure 8: Top: Signal MC efficiencies, relative to the total number of events per SMS point, for the LeptonBVeto (top left), BVeto (top right), and BJet (bottom) boxes as a function of the SMS `T1tttt` model parameters. It can be seen that the signal efficiency in the two data control regions is very low.

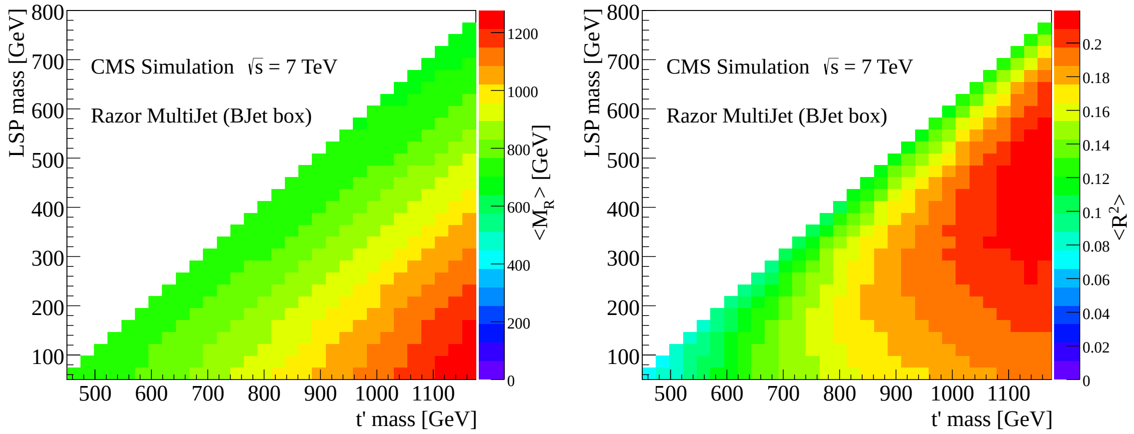

Figure 9: Average values of M_R (left) and R^2 (right) for the BJet box as a function of the SMS `T1tttt` parameters.

References

[1] T. Han, R. Mahbubani, D. G. Walker et al., "Top Quark Pair plus Large Missing Energy at the LHC", *JHEP* **0905** (2009) 117, doi:10.1088/1126-6708/2009/05/117, arXiv:0803.3820.

[2] J. Alwall, J. L. Feng, J. Kumar et al., "Dark Matter-Motivated Searches for Exotic 4th Generation Quarks in Tevatron and Early LHC Data", *Phys.Rev.* **D81** (2010) 114027, doi:10.1103/PhysRevD.81.114027, arXiv:1002.3366.

[3] P. Fileviez Perez and M. B. Wise, "Baryon and lepton number as local gauge symmetries", *Phys.Rev.* **D82** (2010) 011901, doi:10.1103/PhysRevD.82.011901,10.1103/PhysRevD.82.079901, arXiv:1002.1754.

[4] H.-C. Cheng, I. Low, and L.-T. Wang, "Top partners in little Higgs theories with T-parity", *Phys.Rev.* **D74** (2006) 055001, doi:10.1103/PhysRevD.74.055001, arXiv:hep-ph/0510225.

[5] T. Appelquist, H.-C. Cheng, and B. A. Dobrescu, "Bounds on universal extra dimensions", *Phys.Rev.* **D64** (2001) 035002, doi:10.1103/PhysRevD.64.035002, arXiv:hep-ph/0012100.

[6] CDF Collaboration Collaboration, "Search for Production of Heavy Particles Decaying to Top Quarks and Invisible Particles in $p\bar{p}$ collisions at $\sqrt{s} = 1.96$ TeV", *Phys.Rev.Lett.* **106** (2011) 191801, arXiv:1103.2482.

[7] CDF Collaboration Collaboration, "Search for New T' Particles in Final States with Large Jet Multiplicities and Missing Transverse Energy in $p\bar{p}$ Collisions at sqrt(s) = 1.96 TeV", *Phys.Rev.Lett.* **107** (2011) 191803, arXiv:1107.3574.

[8] ATLAS Collaboration Collaboration, "Search for New Phenomena in ttbar Events With Large Missing Transverse Momentum in Proton-Proton Collisions at sqrt(s) = 7 TeV with the ATLAS Detector", *Phys.Rev.Lett.* **108** (2012) 041805, arXiv:1109.4725.

[9] D. S. Alves, M. R. Buckley, P. J. Fox et al., "Stops and MET: the shape of things to come", arXiv:1205.5805.

[10] J. Hubisz, J. Lykken, M. Pierini et al., "Missing energy look-alikes with 100 pb^{-1} at the LHC", *Phys.Rev.* **D78** (2008) 075008, doi:10.1103/PhysRevD.78.075008, arXiv:0805.2398.

[11] C. Rogan, "Kinematics for new dynamics at the LHC", arXiv:1006.2727. CALT-68-2790.

[12] CMS Collaboration, "Inclusive search for squarks and gluinos in pp collisions at sqrt(s) = 7 TeV", arXiv:1107.1279.

[13] CMS Collaboration, "Search for supersymmetry with the razor variables at CMS", *CMS PAS* **SUS-11-008** (2011).

[14] CMS Collaboration, "Search for supersymmetry with the razor variables at CMS", *CMS PAS* **SUS-12-005** (2012).

[15] D0 Collaboration, "Search for squarks and gluinos in events with jets and missing transverse energy using 2.1 fb^{-1} of p anti-p collision data at $s^{(1/2)}$ = 1.96 TeV", *Phys. Lett.* **B660** (2008) 449–457, doi:10.1016/j.physletb.2008.01.042, arXiv:0712.3805.

[16] CDF Collaboration, "Inclusive Search for Squark and Gluino Production in p anti-p Collisions at $s^{(1/2)}$ = 1.96 TeV", *Phys. Rev. Lett.* **102** (2009) 121801, doi:10.1103/PhysRevLett.102.121801, arXiv:0811.2512.

[17] ATLAS Collaboration, "Search for an excess of events with an identical flavour lepton pair and significant missing transverse momentum in $\sqrt{s}$= 7 TeV proton-proton collisions with the ATLAS detector", (2011). arXiv:1103.6208. Accepted by EPJC.

[18] Atlas Collaboration, "Search for squarks and gluinos using final states with jets and missing transverse momentum with the ATLAS detector in sqrt(s) = 7 TeV proton-proton collisions", arXiv:1102.5290.

[19] ATLAS Collaboration, "Search for supersymmetry using final states with one lepton, jets, and missing transverse momentum with the ATLAS detector in $\sqrt{s}$ = 7 TeV pp collisions", *Phys. Rev. Lett.* **106** (2011) 131802, doi:10.1103/PhysRevLett.106.131802, arXiv:1102.2357.

[20] ATLAS Collaboration, "Search for supersymmetric particles in events with lepton pairs and large missing transverse momentum in $\sqrt{s}$ = 7 TeV proton-proton collisions with the ATLAS experiment", (2011). arXiv:1103.6214. Accepted by EPJC.

[21] CMS Collaboration, "Search for new physics with the jets and missing momentum signature at the LHC", *CMS PAS* **SUS-10-005** (2011).

[22] CMS Collaboration, "Search for Supersymmetry in pp Collisions at 7 TeV in Events with Jets and Missing Transverse Energy", *Phys. Lett.* **B698** (2011) 196–218, doi:10.1016/j.physletb.2011.03.021, arXiv:1101.1628.

[23] CMS Collaboration, "Search for new physics with same-sign isolated dilepton events with jets and missing transverse energy at the LHC", arXiv:1104.3168.

[24] CMS Collaboration, "Search for Physics Beyond the Standard Model in Opposite- Sign Dilepton Events at sqrt(s) = 7 TeV", arXiv:1103.1348.

[25] CMS Collaboration, "The CMS experiment at the CERN LHC", *JINST* **3** (2008) S08004, doi:10.1088/1748-0221/3/08/S08004.

[26] A. L. Read, "Presentation of search results: The CL(s) technique", *J.Phys.G* **G28** (2002) 2693–2704, doi:10.1088/0954-3899/28/10/313.

[27] T. Sjöstrand, S. Mrenna, and P. Skands, "PYTHIA 6.4 Physics and Manual; v6.420, tune D6T", *JHEP* **05** (2006) 026, arXiv:hep-ph/0603175.

[28] F. Maltoni and T. Stelzer, "MadEvent: Automatic event generation with MadGraph", *JHEP* **02** (2003) 027, arXiv:hep-ph/0208156.

[29] GEANT4 Collaboration, "GEANT4: A simulation toolkit", *Nucl. Instrum. Meth.* **A506** (2003) 250–303, doi:10.1016/S0168-9002(03)01368-8.

[30] B. Knuteson and S. Mrenna, "BARD: Interpreting new frontier energy collider physics", arXiv:hep-ph/0602101.

[31] N. Arkani-Hamed et al., "MARMOSET: The Path from LHC Data to the New Standard Model via On-Shell Effective Theories", arXiv:hep-ph/0703088.

[32] J. Alwall, P. Schuster, and N. Toro, "Simplified Models for a First Characterization of New Physics at the LHC", *Phys. Rev.* **D79** (2009) 075020, doi:10.1103/PhysRevD.79.075020, arXiv:0810.3921.

[33] J. Alwall, M.-P. Le, M. Lisanti et al., "Model-Independent Jets plus Missing Energy Searches", *Phys.Rev.* **D79** (2009) 015005, doi:10.1103/PhysRevD.79.015005, arXiv:0809.3264.

[34] D. Alves et al., "Simplified Models for LHC New Physics Searches", arXiv:1105.2838.

[35] D. S. Alves, E. Izaguirre, and J. G. Wacker, "Where the Sidewalk Ends: Jets and Missing Energy Search Strategies for the 7 TeV LHC", *JHEP* **1110** (2011) 012, doi:10.1007/JHEP10(2011)012, arXiv:1102.5338.

[36] M. Papucci, J. T. Ruderman, and A. Weiler, "Natural SUSY Endures", arXiv:1110.6926.

[37] B. C. Allanach, "SOFTSUSY: a program for calculating supersymmetric spectra", *Comput. Phys. Commun.* **143** (2002) 305–331, doi:10.1016/S0010-4655(01)00460-X, arXiv:hep-ph/0104145.

[38] A. Djouadi, M. M. Muhlleitner, and M. Spira, "Decays of Supersymmetric Particles: the program SUSY-HIT (SUspect-SdecaY-Hdecay-InTerface)", *Acta Phys. Polon.* **B38** (2007) 635–644, arXiv:hep-ph/0609292.

[39] P. Z. Skands et al., "SUSY Les Houches Accord: Interfacing SUSY Spectrum Calculators, Decay Packages, and Event Generators", *JHEP* **07** (2004) 036, doi:10.1088/1126-6708/2004/07/036, arXiv:hep-ph/0311123.

[40] M. Kramer, A. Kulesza, R. van der Leeuw et al., "Supersymmetry production cross sections in pp collisions at sqrts = 7 TeV", arXiv:1206.2892.

[41] W. Beenakker, R. Hopker, and M. Spira, "PROSPINO: A program for the PROduction of Supersymmetric Particles In Next-to-leading Order QCD", arXiv:hep-ph/9611232.

[42] CMS Collaboration, "Tracking and Primary Vertex Results in First 7 TeV Collisions", *CMS PAS* **TRK-10-005** (2010).

[43] M. Cacciari, G. P. Salam, and G. Soyez, "The anti-kt jet clustering algorithm", *JHEP* **0804** (2008) 063–074, doi:10.1088/1126-6708/2008/04/063.

[44] CMS Collaboration, "Commissioning of the Particle-Flow Reconstruction in Minimum-Bias and Jet Events from pp Collisions at 7 TeV", *CMS PAS* **PFT-10-002** (2010).

[45] CMS Collaboration, "b-Jet Identification in the CMS Experiment", *CMS PAS* **BTV-11-004** (2011).

[46] CMS Collaboration, "Measurements of Inclusive W and Z Cross Sections in pp Collisions at 7 TeV", *CMS PAS* **EWK-10-002** (2010).

[47] CMS Collaboration, "Performance of tau reconstruction algorithms in 2010 data collected with CMS", *CMS PAS* **TAU-11-001** (2011).

[48] W. Verkerke and D. P. Kirkby, "The RooFit toolkit for data modeling", `arXiv:physics/0306116`.

[49] R. J. Barlow, "Extended maximum likelihood", *Nucl.Instrum.Meth.* **A297** (1990) 496–506, `doi:10.1016/0168-9002(90)91334-8`.